



Pulsed laser deposition of vanadium-doped manganese oxide thin films for supercapacitor applications

Dongfang Yang*

National Research Council Canada, 800 Collip Circle, London, ON N6G 4X8, Canada

HIGHLIGHTS

- Vanadium-doped manganese oxide active electrode materials for supercapacitors.
- Pulsed laser deposition of vanadium-doped manganese oxide thin films.
- Pseudo-capacitance performance of vanadium-doped crystalline phase of Mn_2O_3 and amorphous phase of MnO_x .
- Specific current and capacitance determined by electrochemical measurements.

ARTICLE INFO

Article history:

Received 14 August 2012
Received in revised form
5 November 2012
Accepted 20 November 2012
Available online 29 November 2012

Keywords:

Electrochemical capacitor
Supercapacitor
Pulsed laser deposition
Vanadium doping
Manganese oxides
Thin films

ABSTRACT

Thin films of vanadium-doped crystalline Mn_2O_3 and amorphous MnO_x have been grown by the pulsed laser deposition (PLD) process on silicon wafer and stainless steel substrates at different substrate temperatures and oxygen gas pressures. It was found that V-doping level as low as 3.2 atm. % can transform the crystal structure of a crystalline Mn_2O_3 film into a crystalline MnO_2 film. V-doping (up to 10 atm. %) has significantly lowered the specific capacitance of the crystalline Mn_2O_3 films. However, V-doped amorphous MnO_x films did significantly increase the specific capacitance at high CV scan rate as compared with the un-doped MnO_x films and the specific capacitance of V-doped amorphous films increased linearly with the V atomic percentage. At high scan rate of 100 mV s^{-1} , 9.7 atm. % V-doped MnO_x film reached a high specific capacitance value of 95 F g^{-1} indicating that V-doped amorphous MnO_x is good candidate active materials for high energy supercapacitors. The results prove that elemental doping can significantly change the electrochemical properties of MnO_x films.

Crown Copyright © 2012 Published by Elsevier B.V. All rights reserved.

1. Introduction

Metal oxides such as RuO_2 [1,2], MnO_2 [3,4], Co_3O_4 [5,6], NiO [7], SnO_2 [8], Fe_3O_4 [9], and V_2O_5 [10] have been employed as electro-active materials for pseudocapacitors. Those metal oxides typically have several redox states or structures and contribute to the charge storage in pseudocapacitors via fast redox reactions. The remarkable performance of RuO_2 in supercapacitors (exhibits the highest specific capacitance values of 720 F g^{-1}) has stimulated many interests in investigating metal oxide system for supercapacitor applications. The commercial use of RuO_2 in a supercapacitor, however, is limited owing to its high cost and toxic nature. Other simple metal oxides such as manganese oxide usually have some

limitations such as poor electrical conduction, insufficient electrochemical cycling stability, limited voltage operating window and low specific capacitance. Those limitations need to be addressed in order for commercial applications of supercapacitors based on metal oxides. New materials with higher specific capacitance have to be exploited and used. Numerical methods have been used to improve the electrochemical energy storage properties of manganese oxide and other less expensive oxides. Those include increasing its surface area by creating nonporous 3-D structures in oxide particles or thin films, increasing its electronic conduction by mixing with conductive carbon particles or carbon nanotubes/nanofibres, and increasing its specific capacitance by forming composites with conductive polymers or other metal oxides, etc.

Elemental doping of simple pseudo-capacitive metal oxides to form mixed metal oxides has been proven to be an effective way to increase their electronic conductivity, specific capacitance and cyclic durability as demonstrated by numerical studies such as mixed binary systems, Ni–Mn oxide [11], Mn–Co oxide [12,13],

* Tel.: +1 519 430 7147; fax: +1 519 430 7064.
E-mail address: dongfang.yang@nrc.gc.ca.

Mn–Fe oxide [14], Ni–Ti oxide [15], Sn–Al oxide [16], and ternary metal oxides systems, Mn–Ni–Co oxide [17], Co–Ni–Cu oxide [18] and Mn–Ni–Cu oxide [19]. These mixed oxides have shown improved properties as electroactive materials for pseudocapacitors and have shed new lights in this area of research. The objective of the work is to develop the doping recipes for manganese oxides to improve their cyclic durability, electronic conductivity and specific capacitance. In our previous work [12], Co_3O_4 was doped into both amorphous MnO_x and crystalline Mn_2O_3 films. Our experimental results demonstrated that Co(cobalt)-doping can significantly increase the specific capacitance of amorphous MnO_x , reaching the value of 200 F g^{-1} , more than twice the capacitance value of the un-doped amorphous MnO_x films. Our previous results as well as others clearly proved that elemental doping can drastically change the electrochemical properties of manganese oxides, and therefore open new avenues for performance improvement for supercapacitor electrode materials. In this work, another doping element, vanadium (V), was composed with manganese oxides and the structure, surface morphology and pseudo-capacitive properties of the mixed V–Mn oxides will be evaluated and presented in this article.

2. Experimental

2.1. Pulsed laser deposition (PLD) of vanadium-doped manganese oxide thin films

Un-doped and vanadium-doped manganese oxide films were grown on silicon and stainless steel substrates using the PLD technique. The PLD process uses a pulsed laser beam generated by a KrF excimer laser (Lambda Physik LPX-210i) operating at a wavelength of 248 nm and pulse duration of 25 ns. During deposition, the laser beam was introduced into a deposition vacuum chamber (PVD products, PLD-3000) through a quartz window and focused with optical lens onto a target surface to ablate the target and deposit thin film in the vacuum chamber. The laser fluence on the target was adjusted to be $2\text{--}3 \text{ J cm}^{-2}$, while the repetition rate was fixed at 50 Hz. The target used for deposition of the V-doped MnO_x films consisted of a pie-shaped V_2O_5 target piece with different angles mounted on the top of a 3.5-inch circular Mn_3O_4 target disk of 2.5 inch thick (99.9% pure, from K.J. Lesker). The pie-shaped V_2O_5 pieces were prepared by cutting a circular V_2O_5 target disk of 0.125 inch thick (99.9% pure, from K.J. Lesker) into various angles. The laser beam was subsequently ablated on the rotating $\text{V}_2\text{O}_5/\text{Mn}_3\text{O}_4$ hybrid target at various substrate temperatures and oxygen pressures at a rotation speed of 18 rpm to form composite thin films deposited directly on the 3-inch Si(100) [p-type, $\rho = 10\text{--}30 \text{ } \Omega \text{ cm}$, from Polishing Corporation of America] or $20 \text{ mm} \times 30 \text{ mm} \times 1.0 \text{ mm}$ polished rectangular stainless steel 316 substrates. To improve the film homogeneities, the substrates were rotated along the vertical axis at a speed of 35 rpm. Before introducing a Si wafer into the deposition chamber, it was cleaned by acetone, and isopropyl alcohol, and then etched in 2.5% HF acid for 5 min to remove the native oxide. The stainless steel substrates were polished by SiC sand paper of grade 200, 400 and then by Al_2O_3 paste of $0.05 \text{ } \mu\text{m}$ to the mirror-like finish. They were then cleaned by acetone and isopropyl alcohol before being introduced into the deposition chamber. After loading the substrate, the system was pumped down to a base pressure below $3 \times 10^{-7} \text{ Torr}$ using a turbo-molecular pump. The substrate to be coated was facing the target, with a stand-off distance of 8–12 cm. During deposition, substrates were heated, under vacuum, using a programmable non-contact radioactive heater. Oxygen gas pressure was adjusted to 100 mTorr during deposition. A schematic diagram of the PLD system and how to ablate a hybrid target has

been given in previous communication [12]. The un-doped and V-doped manganese oxide films with varying V content were grown on silicon substrates using the hybrid $\text{Mn}_3\text{O}_4/\text{V}_2\text{O}_5$ target that consists of a 3.5 inch diameter pie-shaped V_2O_5 target piece of 15° , 30° and 45° placing on the top of a 3.5 inch circular Mn_3O_4 target at 200°C or 500°C in 100 mTorr O_2 . The film structure was examined by using X-ray diffraction equipment (XRD, Philips, X-Pert MRD) with monochromatized Cu K_α in the $\theta_0\text{--}2\theta$ thin film configuration, where θ_0 was fixed at 0.5° . Their surface morphology and chemical composition was then analysed by a Leo 440 field emission scanning electron microscope (FE-SEM) equipped with a Gresham light element detector and a Quartz XOne EDX system. The reflectance of the films at the ultra-violet (UV) and visible wavelength ranges was measured using a photospectrometer from Scientific Computing International. The thickness of films determined from the reflectance data was in the range of 100 nm–400 nm. The weight of V-doped MnO_x films was calculated by the difference in weight of the coated and the un-coated substrate measured by a highly sensitive balance with precision down to $10 \text{ } \mu\text{g}$.

2.2. Electrochemical characterization

Electrochemical characterization of V-doped and un-doped manganese oxide films grown on stainless steel was performed by cyclic voltammetry (CV) in a standard three-electrode cell with 0.5 M K_2SO_4 neutral aqueous solution as the electrolyte. Strong acidic or strong alkaline electrolytes such as H_2SO_4 or KOH electrolytes were not used because manganese oxide films readily dissolve either in strong acidic or alkaline electrolytes under high potentials [20]. The counter electrode was a platinised platinum wire and the reference electrode was an Ag/AgCl electrode fitted with a salt bridge. The potential was cycled with a Gamry PC3 potentiostat within a potential range $-0.1\text{--}0.9 \text{ V}$ vs. Ag/AgCl at a scan rate of 5, 10, 20, 50 and 100 mV s^{-1} , respectively. This potential range was chosen to ensure that redox processes on V-doped and un-doped manganese oxide films occur homogeneously and reversibly. The test cell configuration was designed such that all the thin-film samples under testing have the same surface area ($\sim 4.6 \text{ cm}^2$) exposed to the electrolyte during electrochemical cycling experiments. This ensures that capacitance of V-doped and un-doped manganese oxides can be compared. The specific current and capacitance of V-doped and un-doped manganese oxide films were calculated from cyclic voltammogram data and the weight of the films.

3. Results and discussions

3.1. EDX characterization of un-doped and V-doped manganese oxide films

The chemical compositions of the V-doped mixed oxide films with varying V contents were investigated by Energy Dispersive X-ray analysis (EDX). Fig. 1 shows a typical EDX spectrum of V-doped manganese oxide excited by an electron beam (5 kV). Peaks for the elements of O, Si, Mn and V were observed and the atomic percentage of constituent elements was calculated from EDX spectrum. The Si peak in EDX spectrum is originated from the substrate and the atomic ratios of Mn and V of various V-doped manganese oxide films deposited at either 200°C or 500°C in 100 mTorr O_2 were determined from EDX spectra and are listed in Table 1. The table shows that the V ions concentration is ranging from 3.3 atm. % to 10 atm. % (atomic percentage of V is the number V atoms over total number of V atoms plus Mn atoms) in the V-doped MnO_x films. The formulas of un-doped and V-doped films determined by EDX were also listed in Table 1.

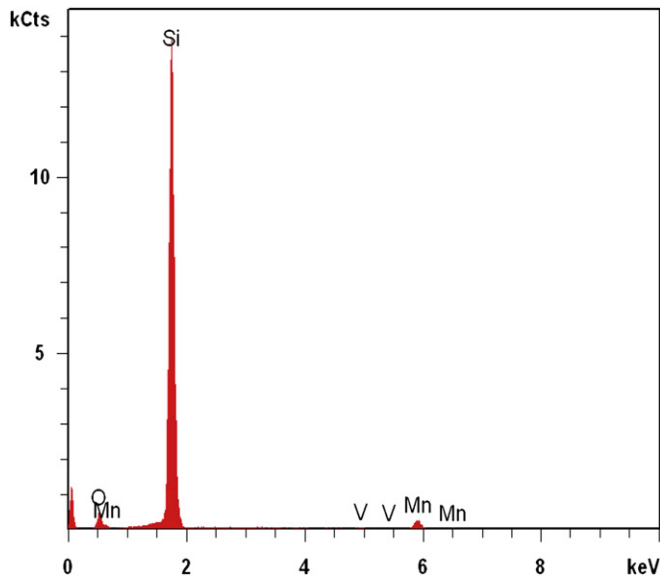


Fig. 1. EDX spectrum of the V-doped MnO_x films deposited by PLD on Si(100) at 500 °C in 100 mTorr O_2 using a 45-degree pie-shaped V_2O_5 target piece mounted on the top of a circular Mn_3O_4 target.

3.2. FE-SEM characterization of V-doped manganese oxide films deposited by PLD

Fig. 2 shows FE-SEM top surface images of un-doped and various V-doped manganese oxide films deposited at 200 °C in 100 mTorr O_2 . The un-doped MnO_x film contains fine grains with grain size of around 30 nm and no pores. Many larger particles of around 50–70 nm in size also emerged on the top of the smooth fine grain structure as shown in Fig. 2(a). When 3.2 atm. % V atoms were doped into the MnO_x film, the grains become very fine with size of around 20 nm and the surface of the film became smoother. The larger particles of around 70 nm size that existed in the un-doped MnO_x film disappeared on the top of the doped film as shown in Fig. 2(b), (c) and (d). When V-doping level increased, the grain size becomes slightly larger but all the doped films still maintain very smooth surfaces.

Fig. 3 shows the FE-SEM top surface images of manganese oxide film and various V-doped manganese oxide films deposited by PLD at 500 °C in 100 mTorr O_2 . The un-doped manganese oxide deposited at high temperature exhibited a smooth and homogeneous structure consisting of very fine grains with grain size of around 20 nm and there were no larger particles appearing on the top of the smooth structure as shown in Fig. 3(a). The fine grains in the high temperature deposited film, however, gathered together to form cluster domains. The fine grains within each domain orientated at the same direction, while fine grains in different

cluster domains oriented in different directions. When low percentage of V (3.3 atm. %) was doped into the manganese oxide film at high temperatures, very fine “oblong-shaped” grains appeared. The low percentage V-doped film is very smooth. As the percentage of V-doping increased to 6.6 atm. % and 10 atm. % as shown in Fig. 3(c) and (d), however, a significant change in microstructure of the film occurred. Spherical fine grains with grain size of around 40 nm appeared in 10 atm. % V-doped film while 6.6 atm. % doped film contained a majority of elongated spherical fine grains. The FE-SEM images in Figs. 2 and 3 clearly showed that V-doping could significantly alter the surface morphology/microstructure of manganese oxide films which eventually will induce change in their pseudo-capacitance behaviours. How the V-doping effect on the crystal structures and electrochemical properties of manganese oxide films will be illustrated in the following sections.

3.3. XRD characterization of V-doped MnO_x films deposited by PLD

XRD patterns of un-doped and V-doped MnO_x films of various V contents deposited on the silicon substrate at 200 °C in 100 mTorr oxygen gas pressure are shown in Fig. 4(a). At substrate temperature of 200 °C, all the un-doped and V-doped MnO_x films are amorphous showing diffuse-scattering curves with very broad and poor-defined peaks centering at 2θ of about 28, 38 and 57°. This is consistent with the FE-SEM results presented in Fig. 2. Those SEM results show that very fine grains of 20–30 nm are the basic consistent units for the low temperature deposited un-doped and V-doped MnO_x films. The relative intense XRD peaks for un-doped MnO_x films comparing to V-doped films is due to its relative larger grains as also shown by FE-SEM in Fig. 2.

When the deposition temperature was raised to 500 °C, well-defined and sharp diffraction peaks appeared for un-doped manganese oxide films as shown in Fig. 4(b). The peak positions of the XRD spectrum of the un-doped MnO_x film matches to either a cubic structure (PDF card #41-1442) or an orthorhombic structure (PDF card #24-0508) [21] of a Mn_2O_3 phase. XRD spectra of all V-doped MnO_x show very weak diffraction peaks and the peak positions are different from the un-doped MnO_x film. Their peak positions match to a tetragonal MnO_2 phase (PDF card #24-0735) [21], indicating that doping of V ions into Mn_2O_3 change its phase (crystal structure). For V ions concentration ranging from 3.3 atm. % to 10 atm. %, the XRD patterns of all V-doped MnO_x films are similar with only their intensity increasing slightly as the V percentage increases and the peak positions do not shift as V-doped level varied. The features in XRD patterns of the V-doped films indicate that when 3.3%–9.7% of Mn ions were substituted by V ion in manganese oxide films, the crystal structure changes from a crystalline Mn_2O_3 phase to a crystalline MnO_2 phase. There are no diffraction peaks originating from V_2O_3 , VO_2 or V_2O_5 phases in the XRD spectra indicating that all V ions are dispersed uniformly into the MnO_2 lattice to form a solid solution. The intensity of XRD peaks for un-doped Mn_2O_3 is higher than the V-doped films since there are grain domains existing in un-doped Mn_2O_3 films in which fine grains are oriented in the same direction. Those same-oriented fine grains in each domain all contributed to XRD peak intensity at the same 2θ angle and “saw” by X-ray just like a large grain having grain size similar to the domain size, although the size of the fine grains that formed the domains in un-doped Mn_2O_3 films is actually smaller than that of the grains in V-doped film. The intensity of XRD peaks of V-doped films decreased significantly which is consistent with change in microstructure as shown in FE-SEM images in Fig. 3. In summary, XRD patterns in Fig. 4 clearly show that V ions were dispersed uniformly into the manganese oxide lattice at 500 °C to replace Mn ions and change its phase structure. The dramatical change in the phase of V-doped MnO_x

Table 1

Atomic ratios of Mn and V for various V-doped MnO_x films deposited by PLD at various conditions.

Process parameters	Target	V atm. %	Formula
500 °C, 100 mTorr O_2	15° $\text{V}_2\text{O}_5/\text{Mn}_3\text{O}_4$	3.3%	$\text{Mn}_{0.967}\text{V}_{0.033}\text{O}_2$
	30° $\text{V}_2\text{O}_5/\text{Mn}_3\text{O}_4$	6.6%	$\text{Mn}_{0.934}\text{V}_{0.066}\text{O}_2$
	45° $\text{V}_2\text{O}_5/\text{Mn}_3\text{O}_4$	10.0%	$\text{Mn}_{0.90}\text{V}_{0.10}\text{O}_2$
	Mn_3O_4	0%	Mn_3O_4
200 °C, 100 mTorr O_2	15° $\text{V}_2\text{O}_5/\text{Mn}_3\text{O}_4$	3.2%	$\text{Mn}_{0.968}\text{V}_{0.032}\text{O}_x$
	30° $\text{V}_2\text{O}_5/\text{Mn}_3\text{O}_4$	6.5%	$\text{Mn}_{0.935}\text{V}_{0.065}\text{O}_x$
	45° $\text{V}_2\text{O}_5/\text{Mn}_3\text{O}_4$	9.7%	$\text{Mn}_{0.903}\text{V}_{0.097}\text{O}_x$
	Mn_3O_4	0%	MnO_x

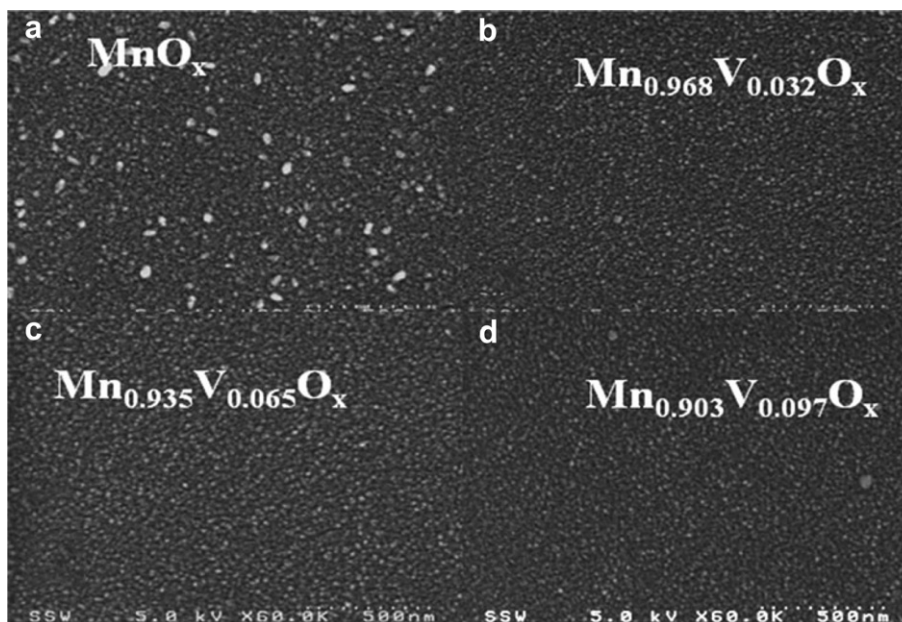


Fig. 2. FE-SEM images of top surface of manganese oxide and V-doped manganese oxide films deposited by PLD at 200 °C in 100 mTorr O_2 : (a) pure MnO_x film, (b) $\text{Mn}_{0.968}\text{V}_{0.032}\text{O}_x$ film, (c) $\text{Mn}_{0.935}\text{V}_{0.065}\text{O}_x$ film and (d) $\text{Mn}_{0.903}\text{V}_{0.097}\text{O}_x$ film.

films are expected to affect their pseudo-capacitance behaviours which will be shown by electrochemical measurements in the following section.

To understand the effect of oxygen gas pressures on the crystal structures of un-doped and V-doped MnO_x films during the PLD deposition process, un-doped and 6.6 atm. % V-doped MnO_x films were deposited by PLD using a Mn_3O_4 target or a hybrid $\text{Mn}_3\text{O}_4/\text{V}_2\text{O}_5$ (30° pie-shaped) target respectively, at 600 °C in 10, 40 and 100 mTorr of oxygen gas pressure and the deposited thin films were

examined by XRD in Fig. 5. XRD patterns in Fig. 5(a) show that under oxygen pressure range of 10–100 mTorr, a pure Mn_2O_3 phase was formed for un-doped MnO_x films deposited at 600 °C. However, when V was doped into manganese oxide films using the hybrid $\text{Mn}_3\text{O}_4/\text{V}_2\text{O}_5$ target at the same condition of 600 °C and 10, 40 and 100 mTorr of oxygen gas pressure, very different crystal structure films were produced. In 40 and 100 mTorr of O_2 , a pure MnO_2 phase was formed, while at low pressure of 10 mTorr, mixed phases of MnO_2 and Mn_2O_3 were formed as shown in Fig. 5(b).

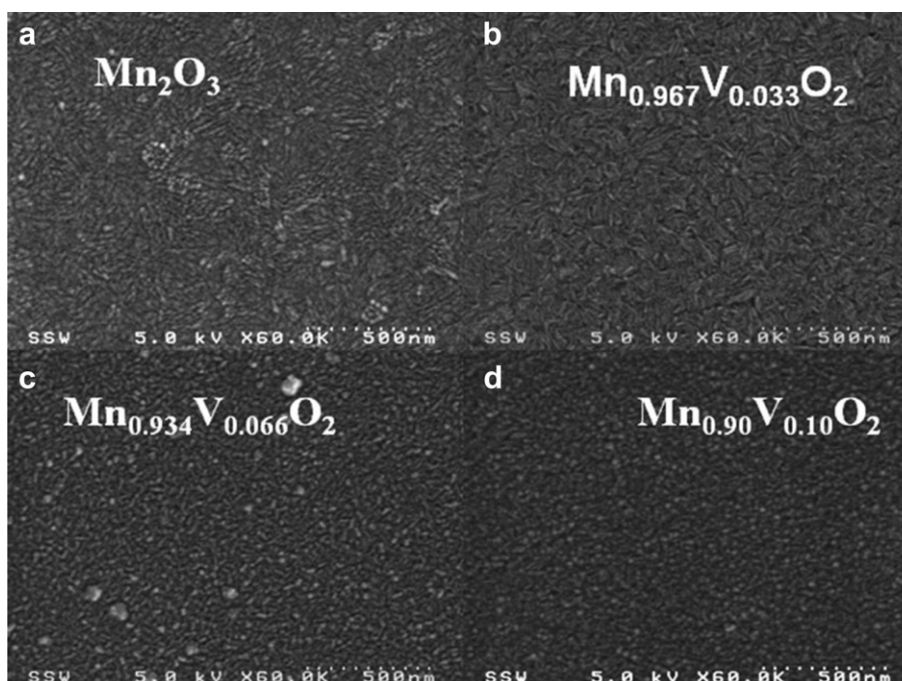


Fig. 3. FE-SEM images of top surface of manganese oxide and V-doped manganese oxide films deposited by PLD at 500 °C in 100 mTorr O_2 : (a) pure Mn_2O_3 , (b) $\text{Mn}_{0.967}\text{V}_{0.033}\text{O}_2$, (c) $\text{Mn}_{0.934}\text{V}_{0.066}\text{O}_2$, and (d) $\text{Mn}_{0.90}\text{V}_{0.10}\text{O}_2$ films.

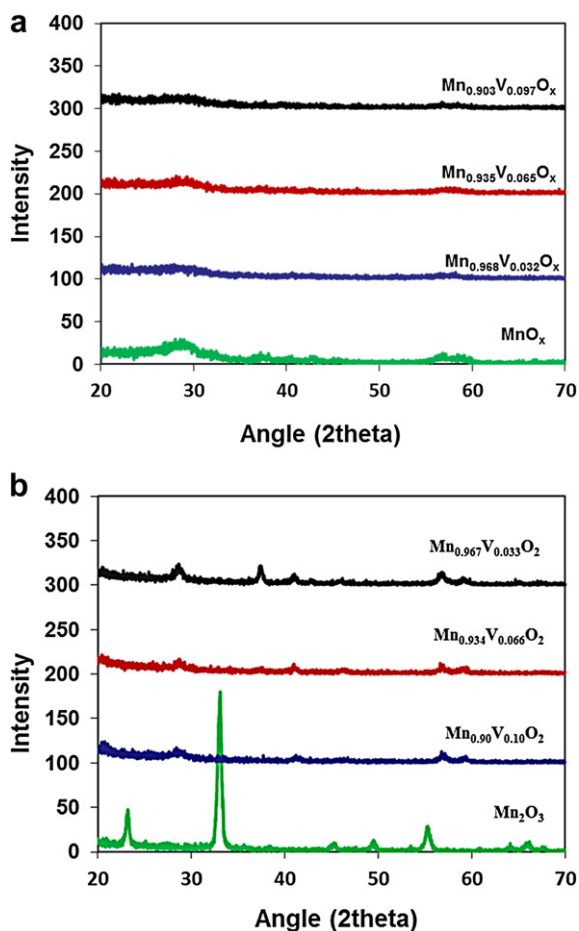


Fig. 4. XRD spectra of un-doped and V-doped MnO_x film deposited by PLD at (a) 200 °C substrate temperatures in 100 mTorr oxygen gas pressures; and (b) 500 °C substrate temperatures in 100 mTorr oxygen gas pressures.

The results in Fig. 5 clearly show that the phase (crystal structure) of MnO_x film can be alternated by both elemental doping and controlling processing parameters of PLD. As pseudocapacitive properties of electrode materials depend on their phases (crystal structures), elemental doping at selected processing conditions provide a new route to generate high performance new electrode materials.

3.4. Electrochemical characterization of V-doped MnO_x films

Electrochemical cyclic voltammetry (CVs) measurements were used to evaluate the effect of V-doping on the pseudo-capacitance behaviours of manganese oxide films deposited both at 200 °C and 500 °C in 100 mTorr O_2 . CVs recorded at 20 mV s^{-1} scan rate for un-doped and various V-doped amorphous MnO_x films deposited at 200 °C by PLD are shown in Fig. 6(a), while their specific capacitance determined from CV curves at scan rates of 1, 10, 20, 50 and 100 mV s^{-1} are shown in Fig. 6(b). The CV and specific capacitance vs. scan rate curves in Fig. 6 show that the V-doped amorphous MnO_x films have larger specific current and capacitance than that of the un-doped amorphous MnO_x film except at the lowest scan rate of 1 mV s^{-1} . High V-doping (9.7 atm. %) has the largest increase in capacitance. The operating potential window (between H_2 evolution and O_2 evolution due to decomposition of water) basically unchanged after V-doping. At the high scan rate of 100 mV s^{-1} , 9.7% V-doped amorphous MnO_x film reaches high specific capacitance

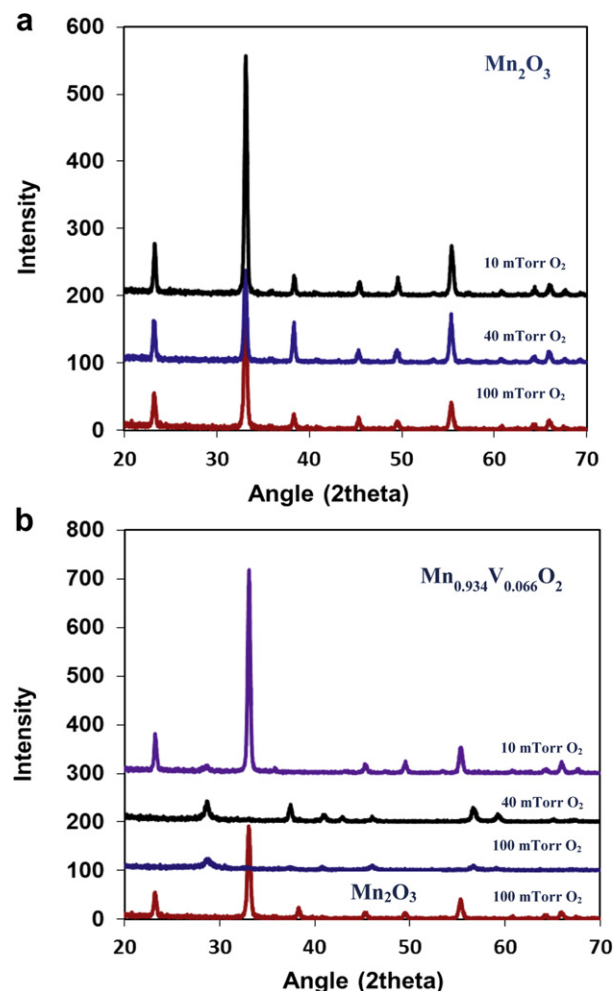


Fig. 5. XRD spectra of (a) un-doped and (b) V-doped manganese oxide films deposited by PLD at 600 °C in various oxygen gas pressures using a Mn_3O_4 target.

value of 95 F g^{-1} indicating that V-doped amorphous MnO_x are good candidate electrode materials for high power supercapacitors. The value of 9.7% V-doped amorphous MnO_x film is 50% more than the value of 64 F g^{-1} for the un-doped MnO_x film, indicating that V-doping can significantly improve the pseudo-capacitance performance of amorphous manganese oxide. However, at the low scan rate of 1 mV s^{-1} , un-doped and various V-doped amorphous MnO_x films have very similar specific capacitance indicating that V-doping may only improve the electrical and/or electrolyte ions conduction in the active layer and do not increase additional redox centers or redox reactions.

The CV and specific capacitance for un-doped and various V-doped crystalline Mn_2O_3 films are shown in Fig. 7(a) and (b), respectively. Doping of V ions into the crystalline Mn_2O_3 film causes its phase transition to the MnO_2 phase as described by XRD characterization. The phase change of the crystalline Mn_2O_3 to MnO_2 significantly reduced the specific current as shown in Fig. 7(a). In Fig. 7(a), the CV recorded at 20 mV s^{-1} scan rate for 10 atm. % V-doped Mn_2O_3 film has higher specific current value than that of the 3.3 atm. % and 6.5 atm. % V-doped Mn_2O_3 films. Similar trend in specific capacitance for un-doped and V-doped Mn_2O_3 films also existed at various scan rates as shown in Fig. 7(b). The specific capacitance of crystalline Mn_2O_3 film reaches as high as 290 F g^{-1} at 1 mV s^{-1} scan rate indicating that crystalline Mn_2O_3 is an excellent electrode materials for high energy supercapacitor, however, its

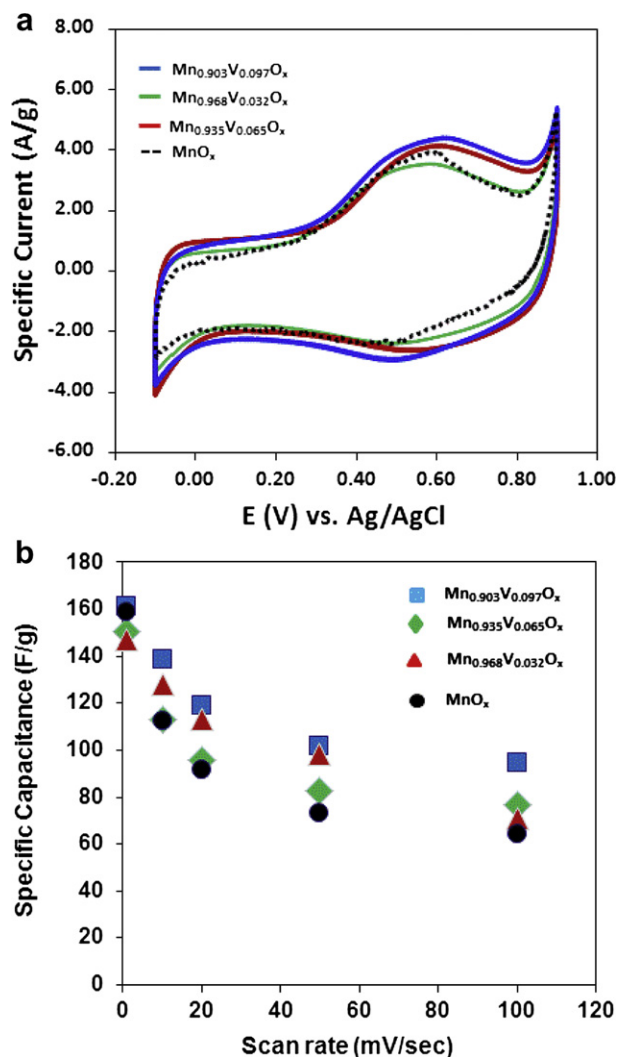


Fig. 6. Cyclic voltammetry (a) and specific capacitance (b) of amorphous MnO_x film and various V-doped amorphous MnO_x films deposited by PLD at 200 °C in 100 mTorr of O_2 .

specific capacitance at high scan rate of 100 mV s^{-1} is relatively low (38 F g^{-1}) indicating that crystalline Mn_2O_3 will not provide same high power value as the amorphous un-doped and V-doped MnO_x films as described previously. However, the relatively low specific capacitance of Mn_2O_3 films at high scan rate may be improved by creating nano-porosity in the film or adding conductive metal particles such as silver.

The effect of atomic percentage of V ions on the specific capacitance of amorphous and crystalline manganese oxide films can be better illustrated in Fig. 8. The specific capacitance values were determined from CVs of the initial first few scans and CVs of scans after many charging–discharging cycles. It can be clearly seen that the specific capacitance of the un-doped and V-doped amorphous MnO_x and crystalline Mn_2O_3 after many charging–discharging cycles is significantly higher than the values determined from initial scans. The reason for the increase in specific capacitance after many charging–discharging cycles could be attributed to the increase in the film roughness (surface area) after charging–discharging cycling. Fig. 8(a) also shows that specific capacitance increases almost linearly with V atomic percentage for the amorphous films and the slopes are $2.8 \text{ F g}^{-1}\text{atm}^{-1} \%$ and $0.8 \text{ F g}^{-1}\text{atm}^{-1} \%$ for initial capacitance and capacitance after long

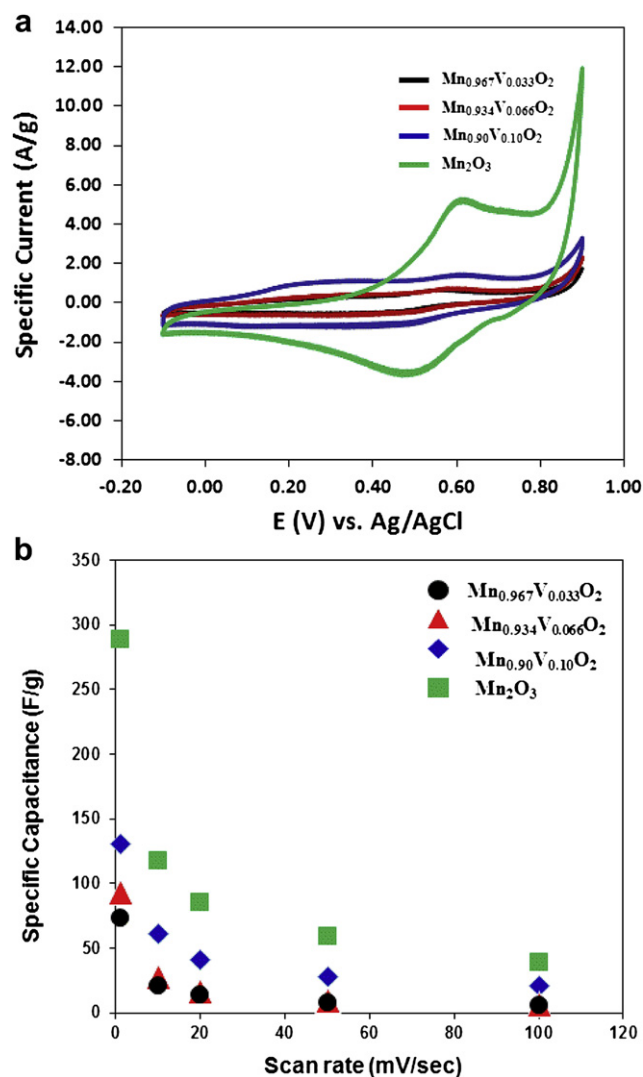


Fig. 7. Cyclic voltammetry (a) and specific capacitance (b) of crystalline Mn_2O_3 film and various V-doped amorphous MnO_2 films deposited by PLD at 500 °C in 100 mTorr of O_2 .

charging–discharging cycles, respectively. Fig. 8(b) shows that when 3.3 atm. % of V was doped into the crystalline Mn_2O_3 film, a big drop in specific capacitance was observed. As XRD spectra in Fig. 4(b) illustrated, doping of 3.3 atm. % of V ions into the crystalline Mn_2O_3 film causes phase change from a crystalline Mn_2O_3 phase to a crystalline MnO_2 phase. The decrease in specific capacitance induced by phase transition implied that crystalline Mn_2O_3 is a better electrode material than crystalline MnO_2 for supercapacitor applications. Further increasing in V atomic percentage from 3.3 atm. % to 10 atm. %, a linear increase in specific capacitance was observed and the slopes are approximately $4.6 \text{ F g}^{-1}\text{atm}^{-1} \%$ for both initial capacitance and capacitance after long charging–discharging cycles. In summary, electrochemical measurements show that doping of V ions into the amorphous MnO_x can significantly improve its pseudo-capacitance while doping of V ions into the crystalline Mn_2O_3 phase cause phase change into a MnO_2 phase and significantly reduced its specific capacitance. The performance of a 9.7% V-doped amorphous MnO_x film reaches very high value of 95 F g^{-1} at 100 mV s^{-1} scan rate indicating that it is a good candidate electrode material for high power supercapacitors.

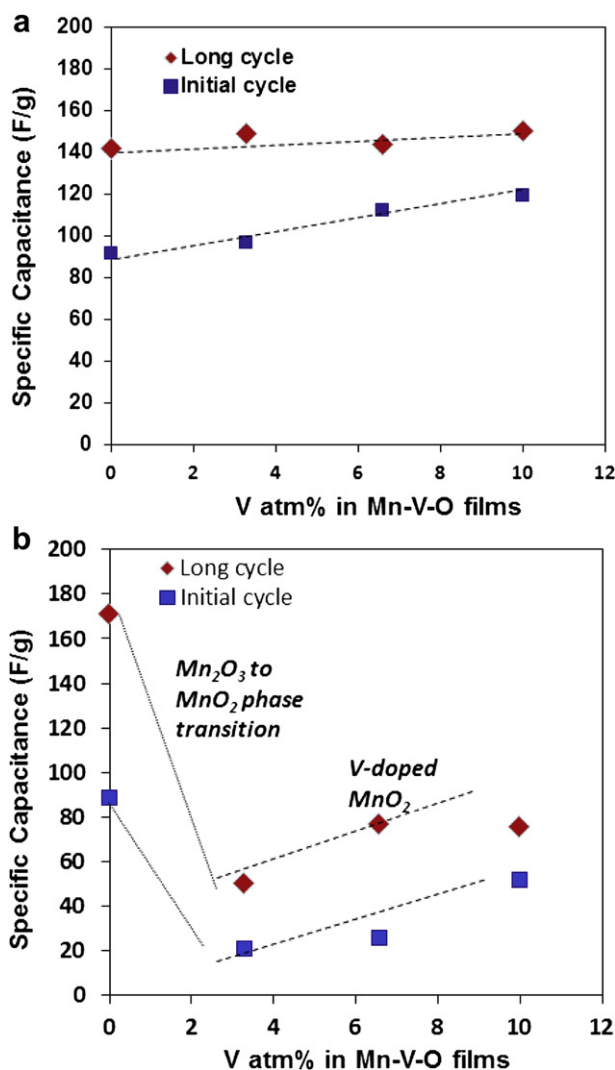


Fig. 8. Specific capacitance vs. V atomic percentage at 20 mV s⁻¹ scan rate for (a) amorphous MnO_x film and various V-doped amorphous MnO_x films, and (b) crystalline Mn₂O₃ film and various V-doped crystalline MnO₂ films deposited by PLD.

4. Discussions

Doping of vanadium into amorphous MnO_x films have been found to increase their specific current and capacitance. At 200 °C and 100 mTorr O₂, which are the conditions used to prepare the V-doped amorphous MnO_x films in this work, stoichiometric V₂O₅ and MnO₂ are expected to be deposited by excimer laser ablation of the hybrid V₂O₅/Mn₃O₄ target. Amana et al. used RBS and XPS to analyse vanadium oxide films produced by excimer laser ablation of a V₂O₅ target over a wide substrate temperature range (30–500 °C) at an oxygen partial pressure of 100 mTorr and found that stoichiometric V₂O₅ were the main composition under these processing conditions [22]. Based on our previous work [23] and analysis, stoichiometric MnO₂ is the main phase that was produced by laser ablation of a Mn₃O₄ target under the same conditions. MnO₂ is known for its poor electrical conductivity of 10⁻⁵–10⁻⁶ S cm⁻¹ which hinder its wide application for supercapacitors with high power performance [24–26]. The electrical conductivity of V₂O₅ dopant has the value of (10⁻²–10⁻³ S cm⁻¹) [27] which is three order magnitudes higher than that of MnO₂. Doping of V₂O₅ into MnO₂, therefore, is expected to increase the electrical conduction of the active materials and eventually its specific capacitance at high

scan rate. This was exactly observed in this work. Actually, V₂O₅ is also one of attractive electrode materials for supercapacitors due to its ease of preparation, low cost and interesting layered structure which has potential to provide fast charging/discharging capacity. Amorphous V₂O₅ was used as the cathode electrode material of supercapacitor both in organic electrolyte [28,29] and in aqueous electrolyte [30,31]. The specific capacitance values of V₂O₅ determined by different research groups in symmetric or asymmetric supercapacitor cells in different electrolytes varied significantly: in a V₂O₅/V₂O₅ symmetric capacitor at a current density of 200 mA g⁻¹ in 2 mol L⁻¹ NaNO₃ solution, the specific capacitance of V₂O₅ was found to be 53.1 F g⁻¹ [32], while the value in an asymmetric supercapacitor cells consisting of activated carbon/V₂O₅•nH₂O nanoribbons in K₂SO₄ aqueous solution reached 180.7 F g⁻¹ [10]. Very high specific capacitance values of 286.3 F g⁻¹ at pH 6.67 and 346.4 F g⁻¹ at pH 2.32 for a-V₂O₅•nH₂O were discovered by Lee and Goodenough [30] in 2 M KCl aqueous solution. T. Cottineau et al. [33] investigated and compared MnO₂, Fe₃O₄ or V₂O₅ oxides for electrochemical supercapacitors working in 0.1 M K₂SO₄ neutral aqueous media. They found that V₂O₅ exhibited the highest specific capacitance values of 170 F g⁻¹ at 2 mV s⁻¹ scan rate, followed by MnO₂ with a value of 150 F g⁻¹ and a smaller value was measured for Fe₃O₄ (75 F g⁻¹). However, they also found the capacitance of V₂O₅ based electrode drastically fades after only a few hundred cycles while MnO₂ and Fe₃O₄ maintained a good specific capacitance after 1000 cycles. In this study, amorphous V₂O₅ was doped into amorphous MnO₂ to form mixed metal oxide nanocomposites, the advantages of utilizing the complementary and synergy behaviours of V₂O₅ and MnO₂ were clearly demonstrated: V-doped amorphous MnO_x films did significantly increase the specific capacitance at high CV scan rate as compared with the un-doped MnO_x films.

Doping of V ions into the crystalline Mn₂O₃ film causes its phase transition to the crystalline MnO₂ phase and significantly reduced its specific current and capacitance. The decrease in specific capacitance when phase transition occurred from Mn₂O₃ to the MnO₂ could due to: i) electronic conductivity change, ii) microstructure change (relating to surface area and double layer capacitance), and iii) Faraday redox reaction rate change (relating to pseudo-capacitance) that associated with the phase transition. Although most of the literature articles suggest that MnO₂ is the best pseudocapacitance materials among all the manganese oxides, our results clearly indicate that crystalline Mn₂O₃ has higher specific capacitance than that of crystalline MnO₂. In our study, highly pure phases of Mn₂O₃ and MnO₂ were successfully prepared by the PLD method to allow such a comparison while most of literature results were taken from mixed and amorphous phases of manganese materials. The increase in V atomic percentage from 3.3 atm. % to 9.7 atm. % in V-doped crystalline MnO₂ films results in a linear increase in specific capacitance with slope of 4.6 F g⁻¹atm.⁻¹ %. The reason for the increase may be attributed to the better electrical conductivity of VO₂ than that of MnO₂. Typical conductivity of VO₂ thin film is 2–5 × 10⁻¹ S cm⁻¹) [34].

Although the specific capacitance values of manganese oxides and V-doped manganese oxides are similar to those of well-known commercially available carbon-based electroactive materials used in electrochemical double layer capacitors, un-doped and doped manganese oxides are of great interest due to their relatively low cost, easily synthesized, and environmentally friendly. By modifying and optimizing their chemical composition, phase and micro/nanostructures, it has great potential to improve their electrochemical behaviours to achieve much higher specific capacitance values than that of carbon-based materials. As one of thin film physical vapour deposition processes, PLD is very useful technique

to prepare simple or complicate metal oxides such as un-doped and doped manganese oxides while precisely controlling their chemical composition, phase and micro/nanostructure, therefore allow for study the composition–structure–property relation of electrode active materials for supercapacitor applications. PLD technique is only used for materials study and will not to be used to produce large quantities of electroactive materials for real supercapacitor devices. The material receipts (composition, phase and micro/nanostructure) revealed by PLD will provide the guideline for other low cost and large quantity processes such as chemical co-precipitation, sol–gel and solid state reactions to reproduce those electroactive materials with similar electrochemical properties like specific capacitance in order for them to be used for real supercapacitor devices.

5. Conclusion

In this work, we have used pulsed laser deposition process to deposit various thin films of V-doped manganese oxides on silicon wafers and stainless steel current collectors at different substrate temperatures and oxygen gas pressures. It was found that V-doping level as low as 3.2 atm. % can transform the crystal structure of a crystalline Mn_2O_3 film into a MnO_2 phase crystalline film. V-doped crystalline MnO_2 films (up to 10 atm. %) have significantly lower specific capacitance than that of the un-doped crystalline Mn_2O_3 films. However, V-doped amorphous MnO_x films did significantly increase the specific capacitance at high CV scan rate as compared with the un-doped MnO_x films and the specific capacitance increased linearly with the V atomic percentage. At high scan rate of 100 mV s^{-1} , 9.7 atm. % V-doped MnO_x film reached a high specific capacitance value of 95 F g^{-1} indicating that V-doped amorphous MnO_x are good candidate active materials for high power supercapacitors. The specific capacitance of crystalline Mn_2O_3 phase at low scan rate is the highest among all the un-doped and V-doped phases indicating that crystalline Mn_2O_3 is an excellent electrode material for high energy supercapacitor. However, its specific capacitance at high scan rate of 100 mV s^{-1} is relatively low (38 F g^{-1}) indicating that crystalline Mn_2O_3 will not provide the same power value as the amorphous un-doped and V-doped MnO_x films. This work has demonstrated that PLD is a very promising technique for supercapacitor material research due to its excellent flexibility and capability of controlling microstructures and phases of various materials. The results also proved that elemental doping can significantly change the electrochemical properties of MnO_x films.

Acknowledgement

The authors would like to thank Transport Canada and National Research Council of Canada's automotive portfolio for supporting this supercapacitors project. The author is also indebted to his NRC

colleagues: Dr. Sylvain Pelletier and Ms. Nathalie Legros for their initiation of supercapacitor research at NRC, and Dr. Alexis Laforge, Dr. Lucie Robitaille, Dr. Yves Grincourt, Dr. Lei Zhang, and Dr. JiuJun Zhang for their collaboration in the supercapacitor research project. He would also like to thank his research team members: Mr. Brian Gibson, Mr. Marco Zeman, Mr. Robinet Romain, Mr. Benjamin Tailpied, and Ms. Gaëlle LEDUC for their dedication to supercapacitor research.

References

- [1] X. Liu, P.G. Pickup, *J. Power Sources* 176 (2008) 410–416.
- [2] C.-C. Hu, K.-H. Chang, M.-C. Lin, Y.-T. Wu, *Nano Lett.* 6 (2006) 2690–2695.
- [3] W. Wei, X. Cui, X. Mao, W. Chen, D.G. Ivey, *Electrochim. Acta* 56 (2011) 1619–1628.
- [4] Y.-C. Hsieh, K.-T. Lee, Y.-P. Lin, N.-L. Wu, S.W. Donne, *J. Power Sources* 177 (2008) 660–664.
- [5] L. Wang, X. Liu, X. Wang, X. Yang, L. Lu, *Curr. Appl. Phys.* 10 (2010) 1422–1426.
- [6] J. Xu, L. Gao, J. Cao, W. Wang, Z. Chen, *Electrochim. Acta* 56 (2010) 732–736.
- [7] A.I. Inamdar, Y. Kim, S.M. Pawar, J.H. Kim, H. Im, H. Kim, *J. Power Sources* 196 (2011) 2393–2397.
- [8] K.R. Prasad, N. Miura, *Electrochem. Commun.* 6 (2004) 849–852.
- [9] N.-L. Wu, S.-Y. Wang, C.-Y. Han, D.-S. Wu, L.-R. Shiue, *J. Power Sources* 113 (2003) 173–178.
- [10] Q.T. Qu, Y. Shi, L.L. Li, W.L. Guo, Y.P. Wu, H.P. Zhang, S.Y. Guan, R. Holze, *Electrochem. Commun.* 11 (2009) 1325–1328.
- [11] E.-H. Liu, W. Li, J. Li, X.-Y. Meng, R. Ding, S.-T. Tan, *Mater. Res. Bull.* 44 (2009) 1122–1126.
- [12] D. Yang, *J. Power Sources* 198 (2012) 416–422.
- [13] J.-K. Chang, W.-C. Hsieh, W.-T. Tsai, *J. Alloys Compd.* 461 (2008) 667–674.
- [14] M.-T. Lee, J.-K. Chang, Y.-T. Hsieh, W.T. Tsai, *J. Power Sources* 185 (2008) 1550–1556.
- [15] Y. Xie, C. Huang, L. Zhou, Y. Liu, H. Huang, *Compos. Sci. Technol.* 69 (2009) 2108–2114.
- [16] M. Jayalakshmi, N. Venugopal, K. Phani Raja, M. Mohan Rao, *J. Power Sources* 158 (2006) 1538–1543.
- [17] J.-M. Luo, B. Gao, X.-G. Zhang, *Mater. Res. Bull.* 43 (2008) 1119–1125.
- [18] T.-C. Wen, H.-M. Kang, *Electrochim. Acta* 43 (1998) 1729–1745.
- [19] D.-L. Fang, Z.-D. Chen, B.-C. Wu, Y. Yan, C.-H. Zheng, *Mater. Chem. Phys.* 128 (2011) 311–326.
- [20] K.-T. Lee, N.-L. Wu, *J. Power Sources* 179 (2008) 430–434.
- [21] Joint Committee on Powder Diffraction Standards, International Center for Diffraction Data, 1996.
- [22] C.V. Ramana, R.J. Smith, O.M. Hussain, C.C. Chusuei, C.M. Julien, *Chem. Mater.* 17 (2005) 1213–1219.
- [23] D. Yang, *J. Power Sources* 196 (2011) 8843–8849.
- [24] Z. Li, Y. Mi, X. Liu, S. Liu, S. Yang, J. Wang, *J. Mater. Chem.* 21 (2011) 14706–14711.
- [25] W. Wei, X. Cui, W. Chen, D.G. Ivey, *Chem. Soc. Rev.* 40 (2011) 1697–1721.
- [26] L. Wei, C. Li, H. Chu, Y. Li, *Dalton Trans.* 40 (2011) 2332–2337.
- [27] F. Coustier, J. Hill, B.B. Owens, S. Passerini, W.H. Smyrl, *J. Electrochem. Soc.* 146 (1999) 1355–1360.
- [28] T. Watanabe, Y. Ikeda, T. Ono, M. Hibino, M. Hosoda, K. Sakai, T. Kudo, *Solid State Ion* 151 (2002) 313–320.
- [29] T. Kudo, Y. Ikeda, T. Watanabe, M. Hibino, M. Miyayama, H. Abe, K. Kajita, *Solid State Ion* 152–153 (2002) 833–841.
- [30] H.Y. Lee, J.B. Goodenough, *J. Solid State Chem.* 148 (1999) 81–84.
- [31] J.-H. Huang, Q.-Y. Lai, J.-M. Song, L.-M. Chen, X.-Y. Ji, *Chin. J. Inorg. Chem.* 23 (2007) 237–242.
- [32] L.-M. Chen, Q.-Y. Lai, Y.-J. Hao, Y. Zhao, X.-Y. Ji, *J. Alloys Compd.* 467 (2009) 465–471.
- [33] T. Cottineau, M. Toupin, T. Delahaye, T. Brousse1, D. Bélanger, *Appl. Phys. A* 82 (2006) 599–606.
- [34] S. Chen, J. Lai, J. Dai, H. Ma, H. Wang, X. Yi, *Opt. Express* 17 (26) (2009) 24153–24161.